

# Constraint Molecular Dynamics approach to Fermionic systems.

Massimo Papa<sup>a,b)\*</sup>, Toshiki Maruyama<sup>a,c)†</sup> and Aldo Bonasera<sup>a)‡</sup>

*a)Istituto Nazionale Fisica Nucleare-Laboratorio Nazionale del Sud, Via Santa Sofia 44, 95123 Catania, Italy*

*b) Istituto Nazionale Fisica Nucleare-Sezione di Catania, Corso Italia 57, 95129 Italy*

*c)Advanced Science Research Center, Japan Atomic Energy Research Institute, Tokai, Ibaraki, 319-1195, Japan*

We propose a Constraint Molecular Dynamics model for Fermionic system. In this approach the equations of motion of wave packets for the nuclear many-body problem are solved by imposing that the one-body occupation probability  $\bar{f}(r, p, t)$  can assume only values less or equal to 1. This condition reflects the Fermionic nature of the studied systems and it is implemented with a fast algorithm which allows also the study of the heaviest colliding system. The parameters of the model have been chosen to reproduce the average binding energy and radii of nuclei in the mass region  $A = 30 \sim 208$ . Some comparison to data is given.

25.70.-z;24.60.-k

## I. INTRODUCTION

Heavy ion collisions in the medium energy region have been described in a large variety of semiclassical approaches to the many-body problem. As it is well known the one-body semiclassical transport models like the Boltzman-Norheim-Vlasov (BNV) [1] and Vlasov-Uehling-Uhlenbeck (VUU) [2] are not suited to describe processes in which a large number of final fragments are produced. This is due to the fact that the correlations treated in the one-body approach are not able to describe the large fluctuations which develops in a multifragmentation process.

This difficulty can be solved by adopting more suitable treatments of the  $N$ -body problem like molecular dynamics. Several molecular dynamics models have been developed up to now [3]. In the quantum molecular dynamics (QMD) [4] the  $N$ -body wave function is expressed through a direct product of wave packets each of which satisfies the minimum uncertainty relation  $\sigma_r \sigma_p = \hbar/2$ , where  $\sigma_r$  and  $\sigma_p$  represent the dispersion of the corresponding Wigner transform in configuration and momentum space respectively.

The Fermionic nature of the nuclear many-body problem has been considered in the Fermionic molecular dynamics [5] and more recently in the antisymmetrized molecular dynamics (AMD) [6]. In these models, the wave function of the system is expressed as a single Slater determinant of  $N$  wave packets. In this way the Fermionic nature of the system is preserved. In particular in the AMD approach two-body collisions are introduced in the “physical coordinates” which are obtained by a canonical transformation from the parameter coordinates of wave-packets [6]. The nucleon-nucleon collision is only allowed when an inverse transformation from a newly chosen “physical coordinate” (the final state of the collision) into the corresponding parameter coordinate exists. This condition is understood as a stochastic change of the state from a single Slater determinant into another, both of which have occupation probability 1 or 0. Due to the four dimensional matrix element of two-body interaction, the CPU time necessary to work out calculations for systems with total mass larger than 200 is very large for practical studies.

On the other hand the QMD calculations are much easier to carry out because they need in general only double-fold loops to calculate two-body interactions. But it is obvious that the Fermionic feature is lacking in the QMD model. Two-body collisions are also introduced phenomenologically. The Pauli blocking of the final state is usually checked in a similar manner to the collision term in the BNV model. The two-body collisions with Pauli blocking have some effects to maintain the Fermionic feature of the system. However, in the ground states or in low energy reaction phenomena, two-body collisions are absent or very rare. Even if the initial state is in good agreement with the phase space distribution of a Fermionic system, the time evolution by the classical equations of motion surely breaks the initial distribution which evolves to a classical Boltzmann one.

To compensate this shortcoming, the Pauli potential is introduced by several authors to mimic the Fermionic features [7–9]. This phenomenological potential forbids nucleons of the same spin and isospin from coming close to each other in the phase space. Although the Pauli potential gives us some good results such as stable ground states,

---

\*e-mail: papa@lns.infn.it

†e-mail: maru@hadron02.tokai.jaeri.go.jp

‡e-mail: bonasera@lns.infn.it

with energies in good agreement with experiments and saturation properties of nuclear matter, it also gave some undesirable by-products, for instance, spurious repulsion in the collision problem.

In the present work we propose a new molecular dynamics model: the Constraint Molecular Dynamics (CoMD), which aims to overcome the above mentioned limitations. In particular we want:

- i) to describe the Fermionic nature of the  $N$ -body system with the more general condition that the occupation probability  $\bar{f} \leq 1$ ;
- ii) to realize a model for which the computational time is short enough to allow the study of the heaviest systems.

## II. THE MODEL

### A. Theoretical framework

In QMD, each nucleon state is represented by a Gaussian wave-function of width  $\sigma_r$ ,

$$\phi_i(\mathbf{r}) = \frac{1}{(2\pi\sigma_r^2)^{3/4}} \exp \left[ -\frac{(\mathbf{r} - \langle \mathbf{r}_i \rangle)^2}{4\sigma_r^2} + \frac{i}{\hbar} \mathbf{r} \cdot \langle \mathbf{p}_i \rangle \right], \quad (1)$$

where  $\langle \mathbf{r}_i \rangle$  and  $\langle \mathbf{p}_i \rangle$  are the centers of position and momentum of  $i$ -th nucleon, respectively. The total wave-function is assumed to be a direct product of these wave-functions. Therefore the  $N$ -body distribution function is the direct product of the single particle distribution functions  $f_i$ . The  $f_i$  are obtained by the Wigner transform of the wave-functions  $\phi_i$  and the one-body distribution function is given by:

$$f(\mathbf{r}, \mathbf{p}) = \sum_i f_i(\mathbf{r}, \mathbf{p}), \quad (2)$$

$$f_i(\mathbf{r}, \mathbf{p}) = \frac{1}{\pi^3 \hbar^3} \cdot \exp \left[ -\frac{(\mathbf{r} - \langle \mathbf{r}_i \rangle)^2}{2\sigma_r^2} - \frac{2\sigma_r^2(\mathbf{p} - \langle \mathbf{p}_i \rangle)^2}{\hbar^2} \right]. \quad (3)$$

We note that since  $\sigma_r$  is a real number in the QMD approach the distribution function  $f_i$  produce the minimum uncertainty relation  $\sigma_r \sigma_p = \hbar/2$  in one-body phase space.

In this paper we extend this kind of representation. We in fact take the dispersion in momentum  $\sigma_p$  as a parameter as well as that in coordinate space allowing for the more general uncertainty condition  $\sigma_p \sigma_r \geq \hbar/2$ . Therefore we write the one-body distribution function as:

$$f_i(\mathbf{r}, \mathbf{p}) = \frac{1}{(2\pi\sigma_r\sigma_p)^3} \cdot \exp \left[ -\frac{(\mathbf{r} - \langle \mathbf{r}_i \rangle)^2}{2\sigma_r^2} - \frac{(\mathbf{p} - \langle \mathbf{p}_i \rangle)^2}{2\sigma_p^2} \right]. \quad (4)$$

This extension implies that each single particle wave function  $\phi_i$  can be now represented by an incoherent superposition of a large number of minimum uncertainty wave-packets.

The equations of motion of  $\langle \mathbf{r}_i \rangle$  and  $\langle \mathbf{p}_i \rangle$  are derived using the time-dependent variational principle which gives:

$$\dot{\langle \mathbf{r}_i \rangle} = \frac{\partial H}{\partial \langle \mathbf{p}_i \rangle}, \quad \dot{\langle \mathbf{p}_i \rangle} = -\frac{\partial H}{\partial \langle \mathbf{r}_i \rangle}. \quad (5)$$

The Hamiltonian  $H$  consists of the kinetic energy and the two-body effective interactions:

$$H = \sum_i \frac{\langle \mathbf{p}_i \rangle^2}{2m} + \frac{1}{2} \sum_{i,j \neq i} \bar{V}_{ij} \quad (6)$$

$$\bar{V}_{ij} \equiv \int d^3 r_i d^3 r_j \rho_i(\mathbf{r}_i) \rho_j(\mathbf{r}_j) V_{ij}, \quad (7)$$

$$\rho_i \equiv \int d^3 p f_i(\mathbf{r}, \mathbf{p}), \quad (8)$$

where  $V_{ij}$  represents two body interaction between particles  $i$  and  $j$  and  $\rho_i$  represents the density distribution of nucleon  $i$ . One should note that the kinetic energy coming from the momentum dispersion  $3\sigma_p^2/2m$  is omitted as a spurious constant term.

## B. Effective interaction

The nucleon-nucleon interaction has been described through the sum of several terms:

$$V_{ij} = V^{\text{vol}} + V^{(3)} + V^{\text{asy}} + V^{\text{sup}} + V^{\text{Coul}} \quad (9)$$

$$V^{\text{vol}} = \frac{t_0}{\rho_0} \delta(\mathbf{r}_i - \mathbf{r}_j) \quad (10)$$

$$V^{(3)} = t_3 \left[ \frac{1}{\rho_0} \delta(\mathbf{r}_i - \mathbf{r}_j) \right]^{7/6} \quad (11)$$

$$V^{\text{asy}} = \frac{a_{\text{sym}}}{\rho_0} \delta(\mathbf{r}_i - \mathbf{r}_j) [2\delta_{\tau_i, \tau_j} - 1] \quad (12)$$

$$V^{\text{sup}} = C_s \nabla_{\langle \mathbf{r}_i \rangle}^2 \delta(\mathbf{r}_i - \mathbf{r}_j) \quad (13)$$

$$V^{\text{Coul}} = \frac{e^2}{|\mathbf{r}_i - \mathbf{r}_j|} \quad (14)$$

In the above relations the power operator  $[..]^{7/6}$  and  $\nabla^2$  act after the folding operations indicated in Eq. (7). The  $\tau_i$  indicates the isospin degree of freedom. The  $V^{\text{vol}}$  and the  $V^{(3)}$  terms represent the two-body and the so called three-body term of the well known Skyrme interaction. The value of  $t_0$  and  $t_3$  have been fixed to  $-356$  MeV and  $303$  MeV. These values reproduce the saturation density  $\rho_0$  and binding energy for symmetric nuclear matter with a compressibility of  $200$  MeV. The third term represent the asymmetry term with  $a_{\text{sym}} = 32$  MeV. The parameter  $C_s$  of the ‘‘surface’’ term  $V^{\text{surf}}$  is chosen through a global fit procedure to reproduce, on the average, the radii and the binding energies for nuclei with mass-ranging from  $30$  to  $208$ .

## C. Numerical methods and the Constraint

The set of equations expressed in Eq. (5) have been solved using a fourth-order Runge-Kutta method coupled with two numerical algorithms which aim to take into account the effects of the residual interaction and the Fermionic nature of the many-body problem we are studying.

One consists of the usual two-body elastic collisions which mimics the effect of the short range repulsive residual interaction together with the stochastic change of the phase-space distribution with Pauli blocking in the final states. The isospin dependent parameterization of the nucleon-nucleon elastic angular distribution together with the concept of mean-free path have been used to compute the collision probability per unit of time [1]. The Pauli blocking factor, which is related to the constraint, is discussed later.

The other algorithm constraints at each time step the following quantities:

$$\bar{f}_i \leq 1 \quad (\text{for all } i) \quad (15)$$

$$\bar{f}_i \equiv \sum_j \delta_{\tau_i, \tau_j} \delta_{s_i, s_j} \int_{h^3} f_j(\mathbf{r}, \mathbf{p}; \langle \mathbf{r}_j \rangle, \langle \mathbf{p}_j \rangle) d^3r d^3p \quad (16)$$

The coordinate  $s_i$  represent the nucleon spin projection quantum number. The integral is performed on an hypercube of volume  $h^3$  in the phase-space centered around the point  $(\langle \mathbf{r}_i \rangle, \langle \mathbf{p}_i \rangle)$  with size  $\sqrt{\frac{2\pi\hbar}{\sigma_r \sigma_p}} \sigma_r$  and  $\sqrt{\frac{2\pi\hbar}{\sigma_r \sigma_p}} \sigma_p$  in the  $r$  and  $p$  spaces respectively. The quantities  $\bar{f}_i$  can therefore be interpreted like an occupation probability of the one-body phase-space around the point of coordinate  $(\langle \mathbf{r}_i \rangle, \langle \mathbf{p}_i \rangle)$ . In general more than 60% of the occupation probability  $\bar{f}_i$  arises from the contribution  $f_i$  of the particle  $i$  itself. To realize the constraint expressed trough the relation (15) the following procedure has been used:

At each time step and for each particle  $i$  an ensemble  $K_i$  of nearest identical particles (including the particle  $i$ ) is determined within the distances  $3\sigma_r$  and  $3\sigma_p$  in the phase space. If the phase space occupation  $\bar{f}_i$  has a value greater than 1 we perform many body elastic scattering among the ensemble  $K_i$  in order to reduce the phase space occupation. To reduce the CPU time the many body scattering process is practically done by a series of two-body scatterings.

The Pauli blocking probability for the usual two-body collision process is given as:

$$P_{\text{block}} = 1 - (1 - S_i)(1 - S_j), \quad (17)$$

$$S_i \equiv \min \left( 1, \frac{\bar{f}_i - \bar{f}_i^i}{1 - \bar{f}_i^i} \right), \quad (18)$$

$$\bar{f}_i^i \equiv \int_{h^3} f_i(\mathbf{r}, \mathbf{p}; \langle \mathbf{r}_i \rangle, \langle \mathbf{p}_i \rangle) d^3r d^3p. \quad (19)$$

The quantity  $S_i$  in Eq. (18) is the “effective occupation” of phase space at the position of particle  $i$ . In fact in the definition of  $S_i$  we are subtracting the contribution of the particle  $i$  itself.

We stress that the constraint acts in a way complementary to the collision term. In fact particles of low momenta are strongly effected by the constraint in such a way to avoid that the distribution becomes a classical one. On the contrary the collision term is especially important for particles located at high relative momenta.

### III. CALCULATIONS AND COMPARISON WITH OTHER MODELS

As an example we compare our results on the isotope distribution in  $^{40}\text{Ca} + ^{40}\text{Ca}$  at 35 MeV/nucleon with the experiment [10] and to the result of QMD. Finally we compare CoMD results to experimental data on central Au+Au collisions [11].

#### A. Initialization

The ground state configuration of the nuclei is obtained using a modified cooling procedure. The nucleon are first distributed in a sphere of radius  $1.4 \times A^{1/3}$  fm in configuration space and in a sphere of radius  $P_F^{\text{nm}}$  (Fermi momentum for infinite nuclear matter) in momentum space. The equations of motion with friction terms are solved coupled with the constraint. At each time step if the value of  $\bar{f}_i$  is greater than 1 the momenta of the particles belonging to the ensemble  $K_i$  are scaled by a factor 1.02. If  $\bar{f}_i$  is less than 1 the scale factor is set to 0.98. With this procedure the total energy and the radius  $R$  of the nuclei will reach some stationary values. If the deviations of these values from the experimental ones are within 7%, a check is done on the stability. At this stage the friction term for the “cooling” is switched off and the time dependence of the nuclear radius  $R$  is checked. If  $R$  is stable at least for 1000 fm/c (inside the confidence level), this initial condition is accepted. In Fig. 1 we show  $R$  as function of time for two typical “good events” representing the  $^{40}\text{Ca}$  and  $^{208}\text{Pb}$  nuclei. The binding energies are  $-8.2$  and  $-8.4$  MeV respectively. The reason of the stability in the CoMD case is the constraint.

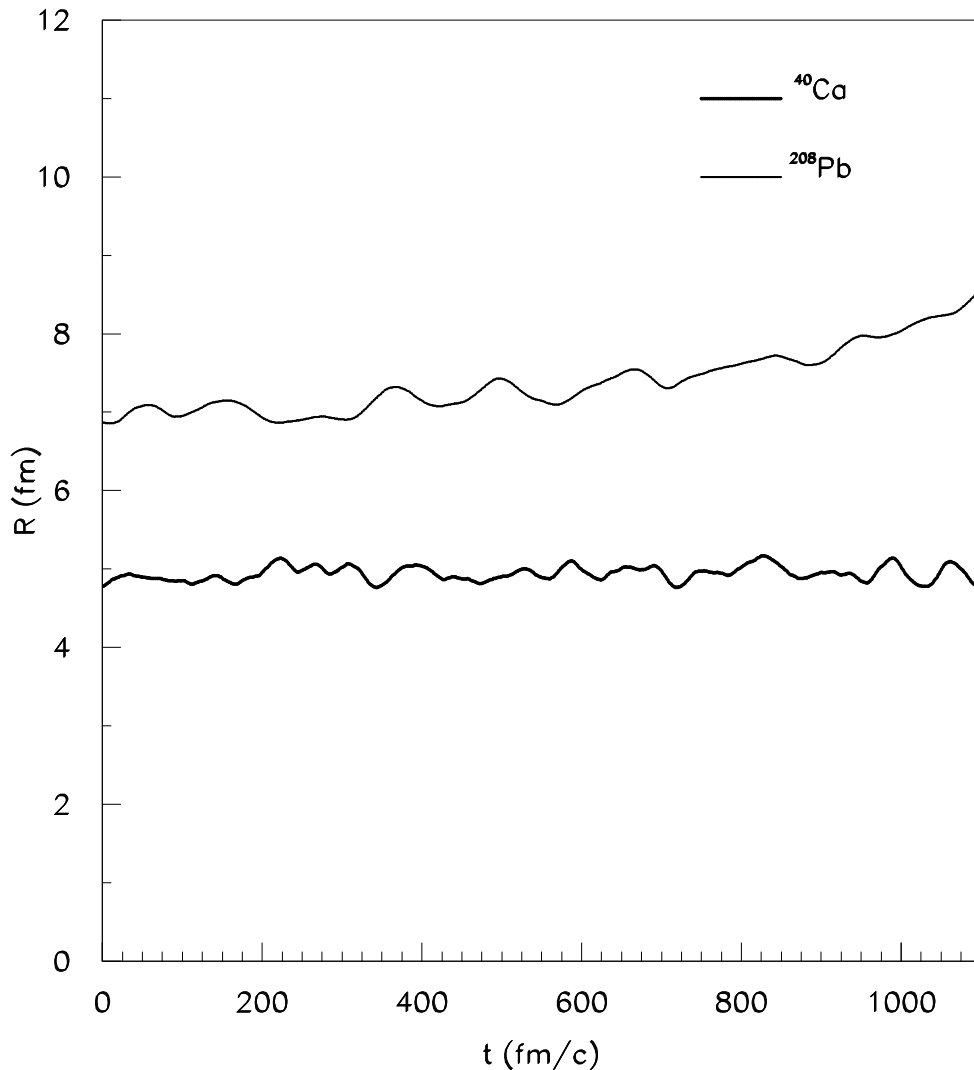


FIG. 1. Nuclear radii  $R$  as function of time for typical ground state configurations of  $^{40}\text{Ca}$  and  $^{208}\text{Pb}$  nuclei.

In fact without constraint, the initial Fermionic distribution will evolve to a classical one. This means that during the interaction several particles will tend to have low relative momenta trying to reach a stable classical configuration (a classical ground state would be a solid) while some other particles (as due to the energy conservation) will acquire momenta large enough to overcome the barrier and leave the system. This does not happen in CoMD since the constraint maintains the Fermionic nature of the system.

The results shown in Fig. 1 are obtained by setting  $\sigma_r = 1.3$  fm,  $\sigma_p/\hbar = 0.47$  fm $^{-1}$  and  $C_s = -2$  MeV $\cdot$ fm $^2$ . The value of the surface term might be surprising at first, but we must notice that part of the surface term comes automatically when using Gaussian. We observe also that using this procedure with the above set of parameters the effective average kinetic energy per nucleon  $K$  (the kinetic energy regarding the centroid of the Gaussian wave packet) is very close to the value obtained in a Thomas Fermi model (about 20 MeV) This feature is instead lost in most of the molecular dynamics models while it is a peculiarity of the proposed one.

In fact in the present approach for a fixed average density and effective interaction, the ratio between kinetic energy and the potential one crucially depends on  $\sigma_p$  which can be varied to values greater than  $\hbar/2\sigma_r$  (see Sec.II). In particular  $\sigma_p$  determines the filling of the phase-space, and therefore, the constrained value of  $\bar{f}$  will be automatically reached with a value of  $K$  strongly depending on  $\sigma_p$ .

This feature will allow us, in the global fit procedure, to find a set of parameters which reproduce the nuclear binding energies, the radii and the ratio between  $K$  and the potential energy close to the value of the Thomas Fermi model.

## B. The Nucleus-Nucleus Collision

In this section we show some results concerning the  $^{40}\text{Ca} + ^{40}\text{Ca}$  collision at  $E_{\text{lab}} = 35$  MeV/nucleon. In Fig. 2 we display the time dependence of  $\bar{f}_i$  for all particle index  $i$  in a typical event with zero impact parameter. The upper and the bottom parts show the results of QMD and CoMD models, respectively, with exactly the same initial condition. The difference between the two cases is quite clear. In the QMD case after a short time (about 50 fm/c) the values of the  $\bar{f}_i$  for most of the particles start to be greater than 1 and are larger than 2 after some hundreds of fm/c. This result is easily understood. In the QMD case, which has no constraint regarding the Fermionic nature except for the two-nucleon collision process, the momentum distribution tends to the classical limit. Obviously in the CoMD case, due to the constraint, the phase space occupation  $\bar{f}_i$  is on the average less than 1 at each time step. We note a good uniformity of  $\bar{f}_i$  as function of the particle index  $i$  and time  $t$ . These results obviously affect the collision rate  $r_c$ .

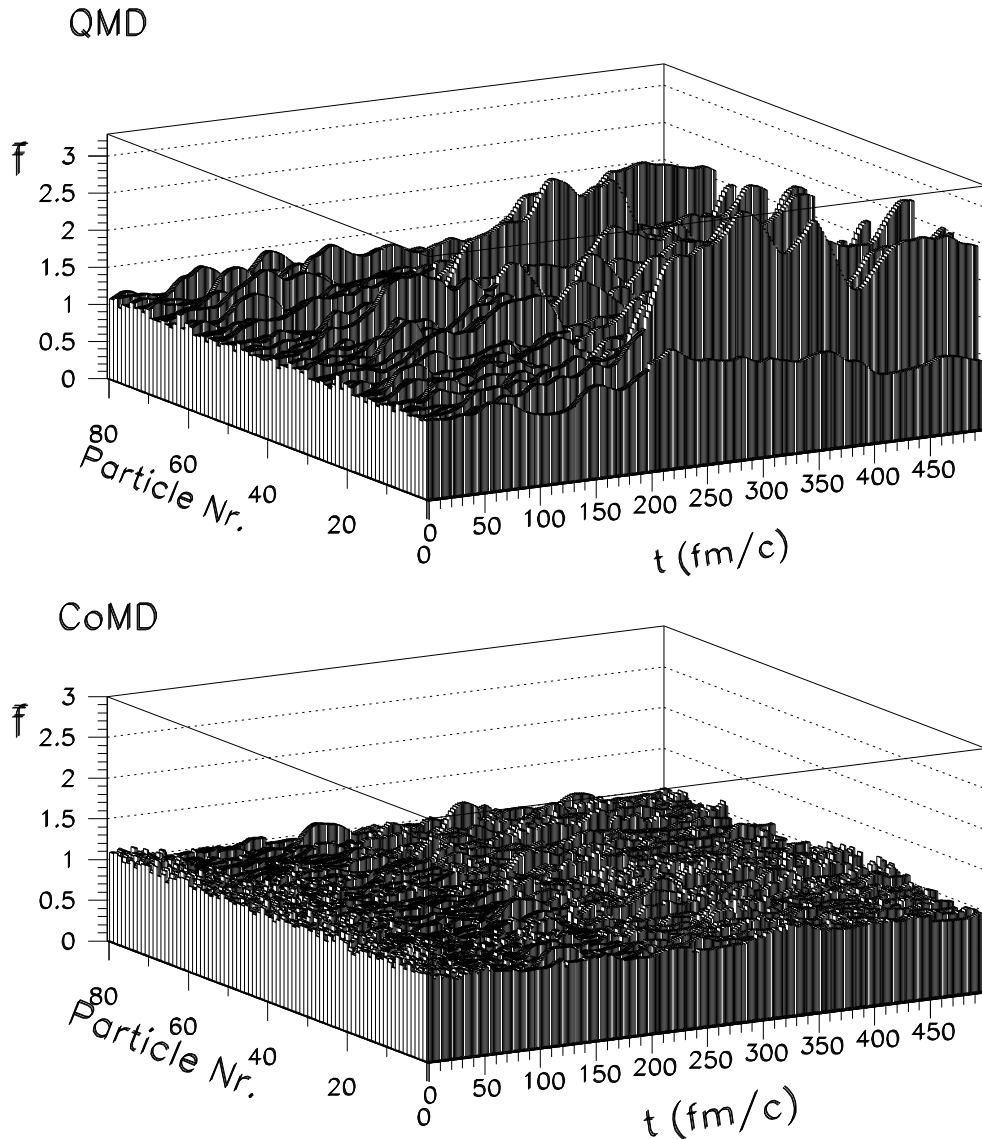


FIG. 2. Two-dimensional histograms showing the occupation probability  $\bar{f}_i$  as function of the particle index  $i$  and time for the system under study. The upper panel refers to the case QMD case while the lower one is relative to the CoMD model.

In Fig. 3 we show  $r_c$  as function of  $t$  for central collision for both the QMD and the CoMD. In the QMD case the collision rate steeply increases and decreases around 40 fm/c. This behavior can be explained as follows: although we

use the same initial condition as CoMD, there appear some fluctuation of occupation number  $\bar{f}_i$  due to the classical nature of QMD. Therefore two-nucleon collisions are easily to occur at the beginning compared to CoMD. After about 30 fm/c, however, when the two nuclei start to overlap the  $\bar{f}_i$  increases spuriously above 1. This causes the rapid decrease of the collision rate in QMD calculations because of the Pauli blocking. The behavior is completely different in the CoMD case. The collision rate develops in about 200 fm/c and reaches a value 3 times greater than the maximum value relative to the QMD case, which in turn gives more stopping. After this time the disassembled system, i.e. the fragments, gradually approach their ground state, which makes the decrease of the collision rate. One may notice, however, the unusually large collision rate even after several hundreds of fm/c. The reason of this large number is due to collisions with very low relative momentum which we do not exclude in the calculations. If some low-momentum cut off of two-nucleon collision is put, we could avoid those high collision rate at later times. Nevertheless those collisions with low relative momentum have no effect on the dynamics.

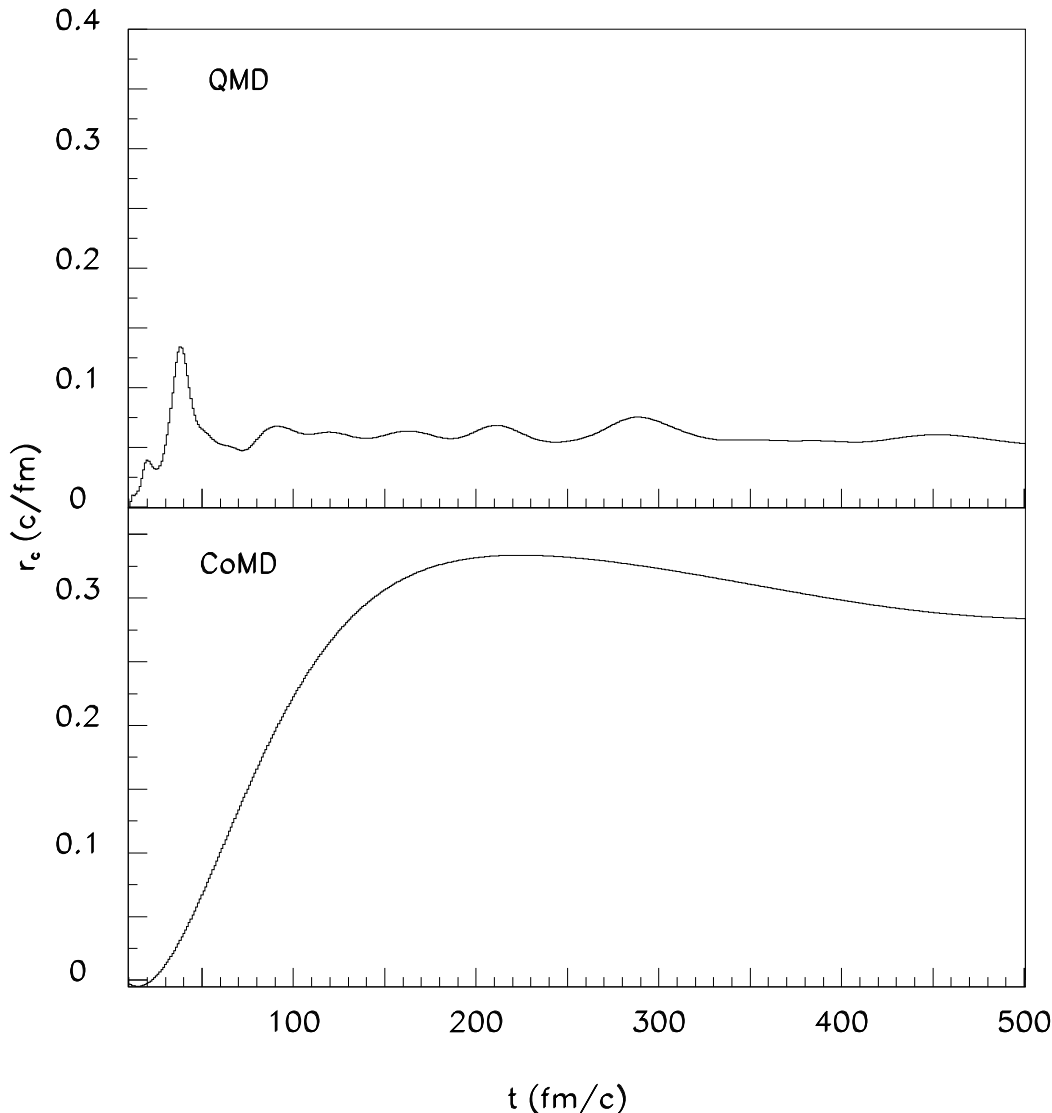


FIG. 3. Collision rate  $r_c$  as function of time for the central collision  $^{40}\text{Ca} + ^{40}\text{Ca}$  at 35 MeV/nucleon in the QMD and CoMD cases.

In Figs. 4 and 5 we compare the isotope distribution given by QMD and CoMD approaches with the experimental data on  $^{40}\text{Ca} + ^{40}\text{Ca}$  [10]. About 2000 events have been generated for an impact parameter range  $b : 0 \sim 8$  fm. The minimum spanning tree method [3] in the configuration space has been applied to determinate the fragments at  $t = 300$  fm/c and at  $t = 3000$  fm/c. We have verified that within the time 3000 fm/c all the fragments are stable. What we can also see from the figure is that the main features of the fragment mass distribution are already

determined at 300 fm/c. After that the process is dominated by the emission of particles from the heavier fragments.

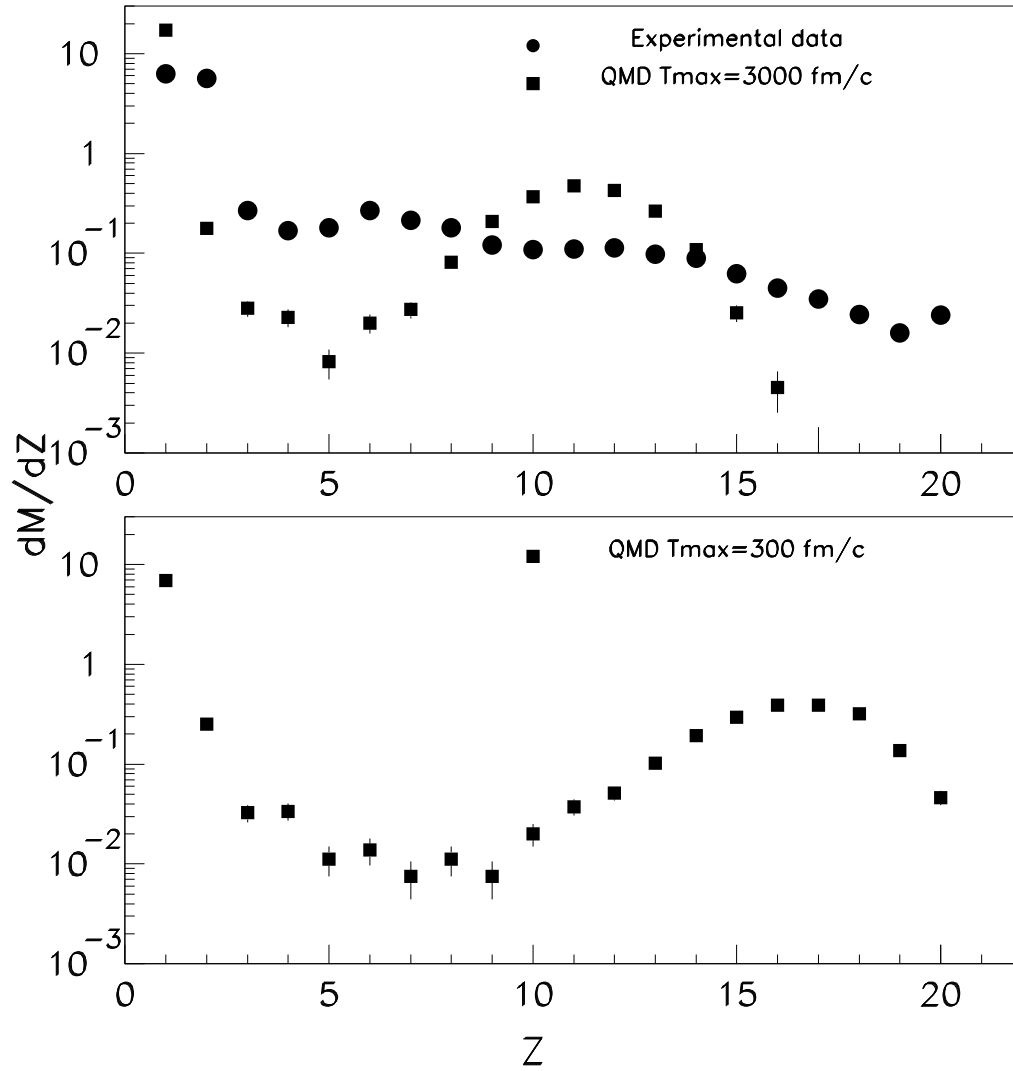


FIG. 4. Comparison between the experimental isotope distribution measured for the  $^{40}\text{Ca} + ^{40}\text{Ca}$  at 35 MeV/nucleon [10] system and the theoretical prediction performed according to the QMD approach. The calculations are shown at two different time intervals as indicated in the figure.

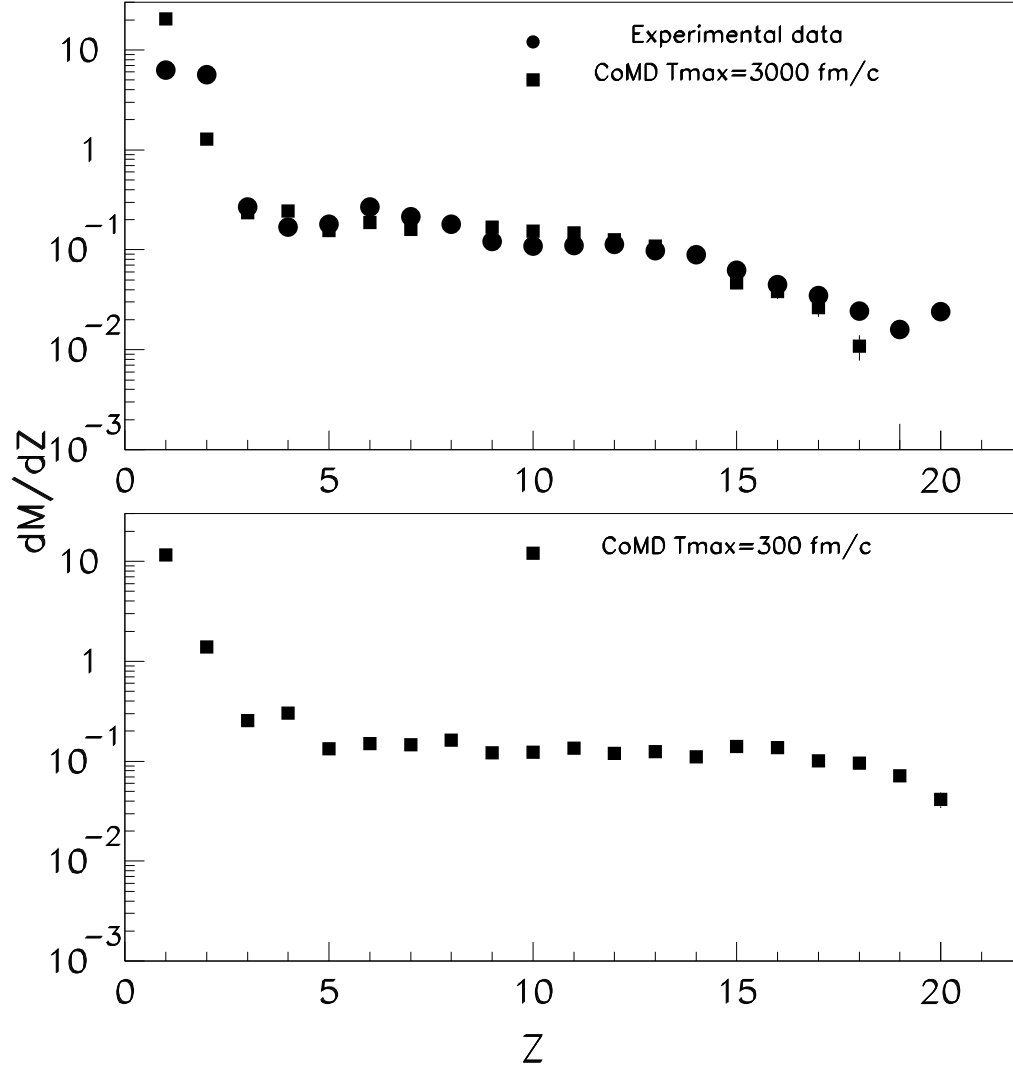


FIG. 5. Same as Fig.4 but for CoMD model.

In the upper panel of Fig. 4 we compare the experimental isotope distribution to QMD at 3000 fm/c. We observe a clear disagreement between the QMD calculation and the experiment. The calculation shows essentially binary character of the reaction while the experimental data shows a significant production of the intermediate mass fragment (IMF:  $Z \geq 3$ ). The binary behavior is due to some kind of transparency obtained in the calculations. This in turn is due to lack of two-body collisions because of the over crowding of the phase space as discussed above. At the bottom of Fig. 4 the result at 300 fm/c is shown. In this case we observe a similar behavior as above, the only difference being a shift of the main bump towards higher value of  $Z$  and a more pronounced “U” shape. In Fig. 5 the same comparison is shown for the CoMD calculation. The calculations are now in a satisfactory agreement with the experimental data. In particular we note that the theoretical prediction of the  $Z = 2$  yield is about a factor ten higher than the QMD case. This is clearly an effect brought by the constraint (15) which favors  $\alpha$  particle states. However the predicted yields of  $Z = 1$  and  $Z = 2$  isotope still show a marked difference with the experimental one.

We have also performed some calculations for the Au+Au system at the same beam energy. Here we are especially interested in central collision. In fact it is quite puzzling the behavior of such a small system but so heavily charged. In Fig. 6 the charge distribution is given for impact parameters up to 3.5 fm and compared to data [11]. A few features are worth noticing.

- 1) CoMD gives too many protons (not displayed in the figure-out of scale).
- 2) The theoretical distribution is slightly shallower than data. Notice however that the data shows a jump for  $Z = 20$  due to the detectors used. If we slightly shift the data yield up for  $Z > 20$  we get a better agreement to the

CoMD results.

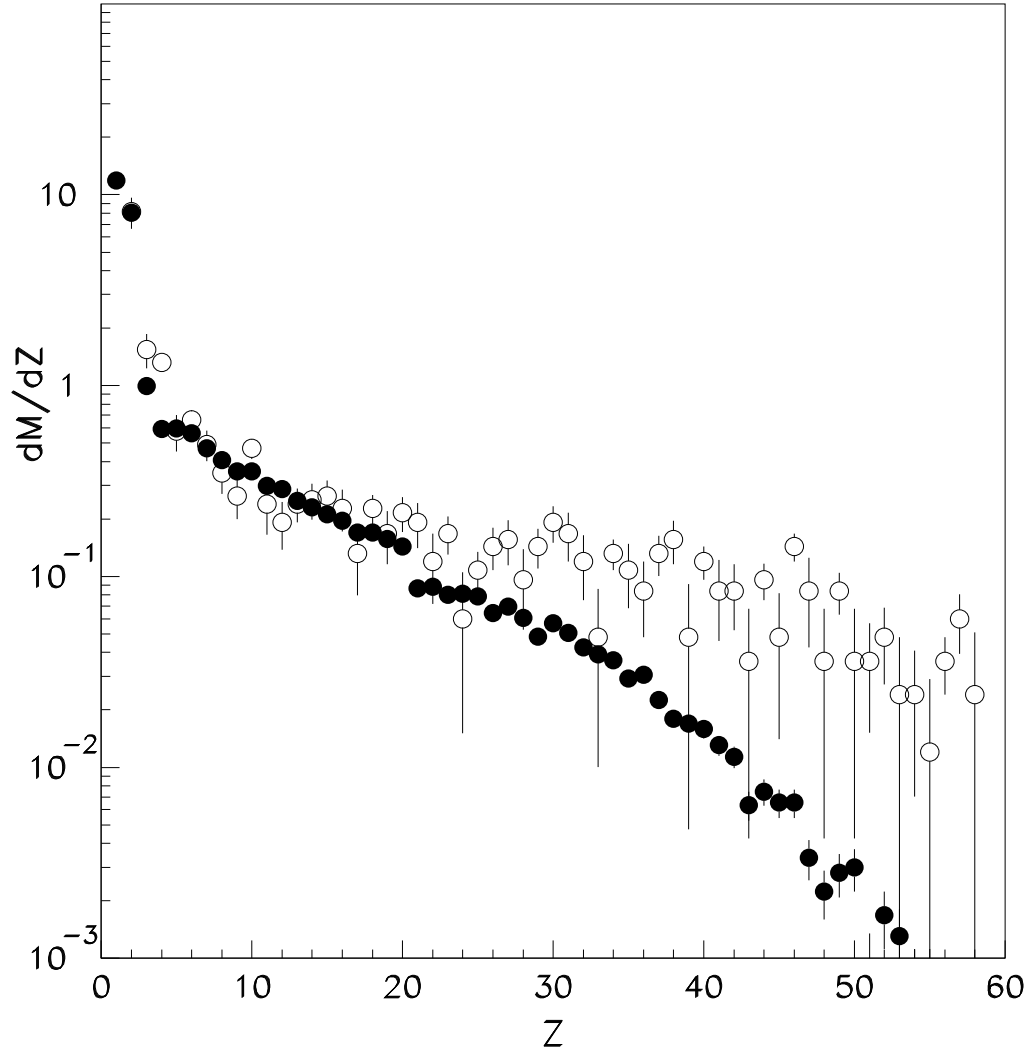


FIG. 6. Comparison between the experimental isotope distribution (full circles)[11] and the calculated one according to the CoMD model (open circles) for central collisions ( $b \simeq 0 \sim 3.5 fm$ )  $^{197}Au + ^{197}Au$  at 35 MeV/nucleon. The vertical bars indicate the errors as due to the statistics counting.

The system was followed up to 1500 fm/c which should be long enough to get cold fragments. Nevertheless we can see from the comparison that the model is working not too bad especially if one recalls that other dynamical model calculations give very steep distributions.

#### IV. CONCLUSION

The CoMD model proposed in the present work is able to reproduce with the same set of parameters both the main characteristic of stable nuclei in a wide region of mass ( $A = 30 \sim 208$ ) and the experimental isotope distribution produced in the collision  $^{40}Ca + ^{40}Ca$  and  $Au+Au$  at  $E_{lab} = 35$  MeV/nucleon. This possibility has a considerable relevance because the above mentioned inclusive information can not be reproduced by the QMD. To this respect the success of the CoMD is due to the constraint represented by the relation (15). This constraint, introduced to describe the Fermionic nature of the nuclear many-body problem, affects the dynamics of the nucleus-nucleus collision for two main reasons:

- a) the nucleon-nucleon collision rate is higher with respect to the QMD case;
- b) the constraint for low momentum particles produces obviously on the average a non local repulsion effect.

Both these effects play a determinant role for the disassembly of the highly excited intermediate systems formed at the beginning of a nuclear collision like that investigated in this work. Finally we stress that for the model proposed the typical CPU time needed to follow the time evolution of systems of mass number around 80 for 300 fm/c is quite short: about 10 sec in a 600 MHz Unix machine.

## V. ACKNOWLEDGEMENT

We thank K. Hagel and M. Dagostino for making their data available to us. A.B. thanks Prof. J. Natowitz for discussions and suggestions. T.M. thanks INFN-LNS for warm hospitality during his stay and M. Colonna for fruitful discussions. Finally M.P. thanks also several experimentalist working at the INFN-LNS for stimulating discussions.

---

- [1] A. Bonasera, F. Gulminelli, and J. Molitoris, Phys. Rep. **243**, 1 (1994).
- [2] G. F. Bertsch and S. Das Gupta, Phys. Rep. 160, 189 (1988).
- [3] A. Bonasera, M. Bruno, C. O. Dorso and P. F. Mastinu, Rivista Nuovo Cimento **23** vol.2, p. 1 (2000)
- [4] J. Aichelin, Phys. Rep. **202**, 233 (1991).
- [5] H. Feldmeier, Nucl. Phys. **A515**, 147 (1990).
- [6] A. Ono, H. Horiuchi, T. Maruyama, and A. Ohnishi, Phys. Rev. Lett. **68**, 2898 (1992)
- [7] L. Wilets, E. M. Henley, M. Kraft, and A. D. Mackellar, Nucl. Phys. A **282**, 341 (1977).
- [8] C. O. Dorso, S. Duarte and J. Randrup, Phys. Lett. B **188**, 287 (1987).
- [9] T. Maruyama, K. Niita, K. Oyamatsu, T. Maruyama, S. Chiba, and A. Iwamoto, Phys. Rev. **C57**, 655 (1998).
- [10] K. Hagel et al., Phys. Rev. **C50**, 2017 (1994).
- [11] P. Desequelles et al., Nucl. Phys. **A633**, 547 (1998).